SSRG International Journal of Electrical and Electronics Engineering
ISSN: 2348-8379/ https://doi.org/10.14445/23488379/IJEEE-V11I9P110
Volume 11 Issue 9, 112-127, September 2024

Original Article

Remote Assistant Technology for Real Time Monitoring of the Agricultural Farmland across the Districts Using Smart Positioning IoT

Sumalatha Aradhya

Department of Computer Science and Engineering, Siddaganga Institute of Technology, Karnataka, India.

Corresponding Author : sumalatha@sit.ac.in

Received: 05 July 2024 Revised: 07 August 2024 Accepted: 05 September 2024 Published: 28 September 2024

Abstract - *Precision agriculture, land surveys, and positioning measures are useful to society for accurate mapping of boundaries in the local agricultural area. An existing approach uses Global Navigation technologies with a deviation accuracy of 10% with geo fencing mechanism. However, a Navigation system needs the support of advanced positioning technology to improve positioning accuracy. In the paper, a novel approach to positioning is proposed. The approach includes a digital classification and optimization of area mapping, enhancement of correlation data, analysis through an expert system and clustering of delineation zones using an optimized Artificial Bee Colony algorithm. Precision accuracy is achieved by the correction of zonal map boundaries and radio frequency sensors. The real time kinematics technique is applied further to do the deviation corrections, improvement, and optimization. An experiment was carried out in real time between two districts, namely Bangalore and Tumakuru, where the distance was nearly 60 km. An optimized artificial bee colony algorithm is used to correct errors and improve positioning accuracy. The real time field trail data is analyzed, calibrated, and improved further to obtain a precision accuracy of 99.9%.*

Keywords - *Precision accuracy, Remote sensing, Real time kinematics, IoT, Satellite navigation, Localization, Delineation, Positioning, Assistant technology.*

1. Introduction

The Satellite Geospatial data is obtained from the remote sensing device that has the raw GNSS data in WG84-based format [1]. The raw GNSS data is humungous, and data is generated dynamically within a millisecond. The extraction of NGS CORS data from the generated data is challenging and requires an optimal algorithm [2, 3]. After the data acquisition, data processing and data transformation are to be performed further by using ML/DL based algorithms [4-6]. Precision agriculture needs accuracy in the creation of management zones [7]. The Kriging interpolation method, though, gives the solution. Precision accuracy is still a challenge in agriculture, Land Survey, and other field specific applications [8]. Real Time Kinetics (RTK) is the mechanism used for deriving positioning accuracy in any area or zones [9, 10]. However, positing accuracy is still a challenge in real time. An IoT-based approach is needed to monitor the farmland area where the distance between the source and end node is more than 50km. The proposed solution uses the RTK based solution to determine the accuracy of GNSS positioning using an IoT kit.

Considering the diversion of the points of projections, one needs to map the directions across the dimensions of coordinate systems. The spectral difference between the coordinate points interprets the accuracy level of the projection points [11]. Point level fusion mapping can be done to extract the coherent information of coordinates and then apply the decision rules to obtain new coordinate projection space [12]. Real time kinetics can be used in IoT applications such as smart cities, agriculture, environment, robotics, autonomous vehicles, etc. [13].

Real-time kinetics gives the positioning references using fixed and movable reference stations [14]. Real time kinetics works with dual frequency, and it mitigates positioning errors by differentiating the positions between the reference station and the movable station. In Vietnam and other European countries, dual frequency based real time kinetic measurement technique is used [15, 16]. With optimized real time kinetics protocol implementation through the GNSS receiver and NTRIP caster framework, precision accuracy is possible [17]. A similar approach is incorporated in this paper with optimization in real time kinetics. The trajectory planning method is used in Unmanned Aerial Vehicle delineation. A Trust Region Filtered Sequential Convex Programming is proposed to build UAV trajectories [18]. The image fusion space with geo plots needs projection mapping calculations and involves complicated computations [13]. Mixed Integer Linear Programming. To solve the trajectory planning problem, the interpretation of Random Tree Exploration and Informatics can be used [19]. The computation methods and algorithms logics increase the complexities of plotting the trajectories [20]. Convex programming methods are suggested for improving the trajectory generation [12, 17].

Comprehensive Analysis is needed to achieve geo fencing through China's BDS-3 based carrier shift methods for range specific GNSS data [21]. Tukey and K-Means methods are suggested by Massimiliano et al. to implement Single Point Positioning on GIS applications [22]. Determining spatial differentiation of geographical areas using Ecological Redline Area is proposed by Deng Sui Chen et al. [23]. Trial and error-based methods are followed in actual model scaling analysis to develop tractable simulations [24].

A polynomial model is a common method for geometric correction. The order of the polynomial and remote sensing is not co-related, and hence, machine learning algorithms such as the ENVI deep learning model are proposed by Weicheng Xu et al. [25]. Imperative areas are detected through down-sampled Global Nighttime Light using multi-source spatial variables as proposed by Yang Ye et al. [26]. However, accuracy up to a cm level is not achieved, and hence, a unique approach that integrates RTK, GNSS and RFID sensors is proposed in the paper.

2. Related Work

A limited amount of work was found in the Smart Positioning IoT in the farmland area. The existing method uses a Geographic Information System to locate the positioning area of farmland. The Real time kinematics approach is found in European urban areas and is not used much in Asia-specific countries. Section 2.1 gives the existing approach using GIS. Section 2.2 illustrates the existing approach using RTK, and Section 2.3 gives insight into the existing approach that combines both GIS and RTK along with the IoT framework.

2.1. GIS Based Information

Precision accuracy for Galileo constellation positioning can be determined by single frequency modeling and computation as proposed by Bahadur, B [13]. Post Processing Kinematics and Real Time Kinematics are the methods suggested to achieve accuracy in unmanned vehicles, and the outcome shows that a Root Mean Square of 0.0189m is achieved by Nicola et al. and the team [14]. Multi-spectrum Instrument-based satellite positioning data on the land area was studied, and the solution to spatial variability is discussed in Mortz K. Lehmann et al.'s paper [27]. Monitoring forest areas based on multi-source remote sensing by observing phenological surfaces of the environment was studied by Yali Zhang et al. [28]. A sequence of extraction of points using a Gated Recurrent Unit framework and neighbor network hood algorithm is proposed by Yi He et al. [29]. Horizontal coordinate points for the transformation of points in the longitudinal axis of the original coordinate system can be computed by using the gradient component derivation method as proposed by Andreas A. Beckert et al. [30]. Satellite images are analyzed through remote sensing computations using an optimized algorithm suggested by Hu et al. [31].

High powered trajectory optimization to provide tri-axis commands and an attitude control approach is proposed by Mazinan et al. [32]. However, scale-dependent spatial pattern quantification is challenging and needs power law predictions, as proposed by Qun Ma et al. [33]. By backtracking the traces of encroachment space patterns across the Southern Great Plain, a threshold value for accuracy assessment was studied by Xuebin et al. [34]. It has been proven that the utilization of GIS-based methodologies is needed in various regions, zones, and other areas [35]. The delineation of land area may not be accurate at all locations [17, 36].

Bumairiyemu Maimaiti et al. suggested mapping classifications, expansion scaling, and relevant parameter calculations through ArcGIS software [37]. Diversified land zones and mapping of the areas through consistent characterization with an accuracy of 4.77m is implemented by Yang, F. and Zeng, Z. [38]. An intense investigation was conducted, in the mountain region of Asia, where complexities are high due to unstable slopes. The investigation focuses on the localization of mountain regions with geo marking. However, a cm level accuracy is not achievable with the GIS-based approach alone.

2.2. Real Time Kinematics Technology

In urban areas, the GlobalUrbanNet-based framework is useful, as proposed by Yanfei Zhong et al. and team in their work [39]. Taddia Y et al. proposed Network RTK and DJI Phantom RTK modes to achieve GNSS accuracy and achieved a 5cm offset with vertical residuals [40]. The optimization technique is needed to improve the harmonic response and analysis of the antenna to be performed. A monopole antenna is analyzed, and mitigations are proposed by Jadon et al. [41] and Chand P S P et al. [42].

A wireless sensor testbed to record the metadata and calibrate the timestamp according to the recorded data segment is useful as a default gateway [48]. Several contiguous coordinate frame data are resampled, interpolated and modelled to achieve approximation values needed for accuracy [49-54]. An unlimited sensing framework-based method was proposed for radar signal radiation based application. The radar signal radiation approach is not suggested for farmland area monitoring as an inherited complexity of technology is needed in real time.

A real time kinematics approach is proposed in this paper to achieve an offset accuracy of 2mm. The proposed IoT application is novel and is useful in use cases such as agriculture precision management, real time object tracking management and safety critical applications and management.

2.3. IoT System with GNSS and Real Time Kinematics

An autonomous vehicle's tracking system is proposed based on prediction control [55]. However, precision accuracy on positioning is not attained. Backstepping sliding mode control is proposed in the work to track the robot. Though kinematics is used in the model, the positioning measures are not clear.

In UWB-based e Saleh- Valenzuela method, the solution works for indoor area localization, and the experiment was carried out using Matlab based simulation environment rather than real time. The cluster head selection method is suggested by Ahmed Salim et al. for smart city data collection on IoT-based Wireless Sensor Networking systems [56]. Denes Farago et al. propose the calibration coefficient with the continuous detection of stationary data. However, precision measures are compared with Matlab, LabView, and non-iterative methods, not real time [57].

Next Generation Positioning, NGP, is used in a centimeter level approximation of Wi-Fi ranging with a median 2.7 cm error [58]. The accurate line of sight signal method is proposed by Ying Zhang et al., and real time reconstruction of positioning data is difficult as correction time is more [59]. Jiale Wang et al. suggest a 3D mapping precise point positioning and accuracy with meter level is achieved [60]. It is proven that precision positioning accuracy is achievable with absolute and relative positioning solutions in GNSS denied atmosphere [61]. A more precise method is needed in a GNSS-based environment.

GPS integrated RFID antenna with an artificial magnetic conductor device is used for IoT based tracking applications by Chandni Bajaj et al. [62]. It is suggested that the high-impedance antenna be used for better results. In our work, we have proved that positioning accuracy using radio frequency receivers integrated with real time kinematics provides better results. With resampling, interpolation through patch antenna, and the application of an optimized machine learning algorithm, the artificial bee colony algorithm, one can correct the misalignment and distortion. Furthermore, error correction and modeling can be done with the optimized computational procedure or technique.

The real challenge of engineering a complex system is to aggregate the electric, electronic, mechanical, and computing elements. The tool simulations or modeling is needed to study and analyze the behavior and performance of the elements. Signaling strength, gain, and better impedance with low cost were needed to derive a delineation solution in the first place. The optimization technique is needed to improve the harmonic response and analysis of the antenna to be performed. Signaling strength, gain and better impedance with low cost were needed for deriving a delineation solution in the first place. The different types of radio frequency antennas are listed in Figure 1.

3. Materials and Methods

The optimization technique is needed to improve the harmonic response and analysis of the antenna to be performed. The Patch family of the antenna is considered for our work, and the manufacturer patch family antenna is depicted in Figure 2. The distribution of each of the patch family antenna is analysed further to determine an efficient source for the signal. The distribution of antenna coverage is shown in Figure 3. It is evident from the pattern analysis that the microstrip antenna with patch inset fed antenna is efficient and can be used in the proposed system to improve the accuracy.

1. Dipole Family

1. Dipole Antenna
2. Folded Antenna
3. Vee Antenna
4. Meander Antenna
5. Bowtie-Triangular Antenna
6. Bowtie-Rounded Antenna
7. Blade Antenna
8. Cycloid Antenna
9. Jpole Antenna

2. Fractl Family

1. Gasket Antenna
2. Koch Antenna
3. Island Antenna
4. Carpet Antenna
5. Snow Flake

3. Helix Family

1. Helical Dipole Antenna
2. Helix Antenna
3. Multifilar Diploe Antenna

4. Loop Family

1. Circular Antenna
2. Rectangular Antenna

5. Spiral Family

1. Spiral Archimedean Antenna
2. Equiangular Antenna
3. Rectangular Spiral Antenna

6. Patch Family

1. Micro Strip Antenna
2. Pifa Antenna
3. Inverted F Coplanar Antenna
4. Inverted L Coplanar Antenna
5. Patch Micro Strip Inset Fed Antenna
6. Patch Micro Strip Circular Antenna
7. Triangular Patch Antenna
8. E-Patch Antenna
9. H-Patch Antenna
10. Elliptical Antenna

Fig. 1 Experiment target list of antennas [41, 63]

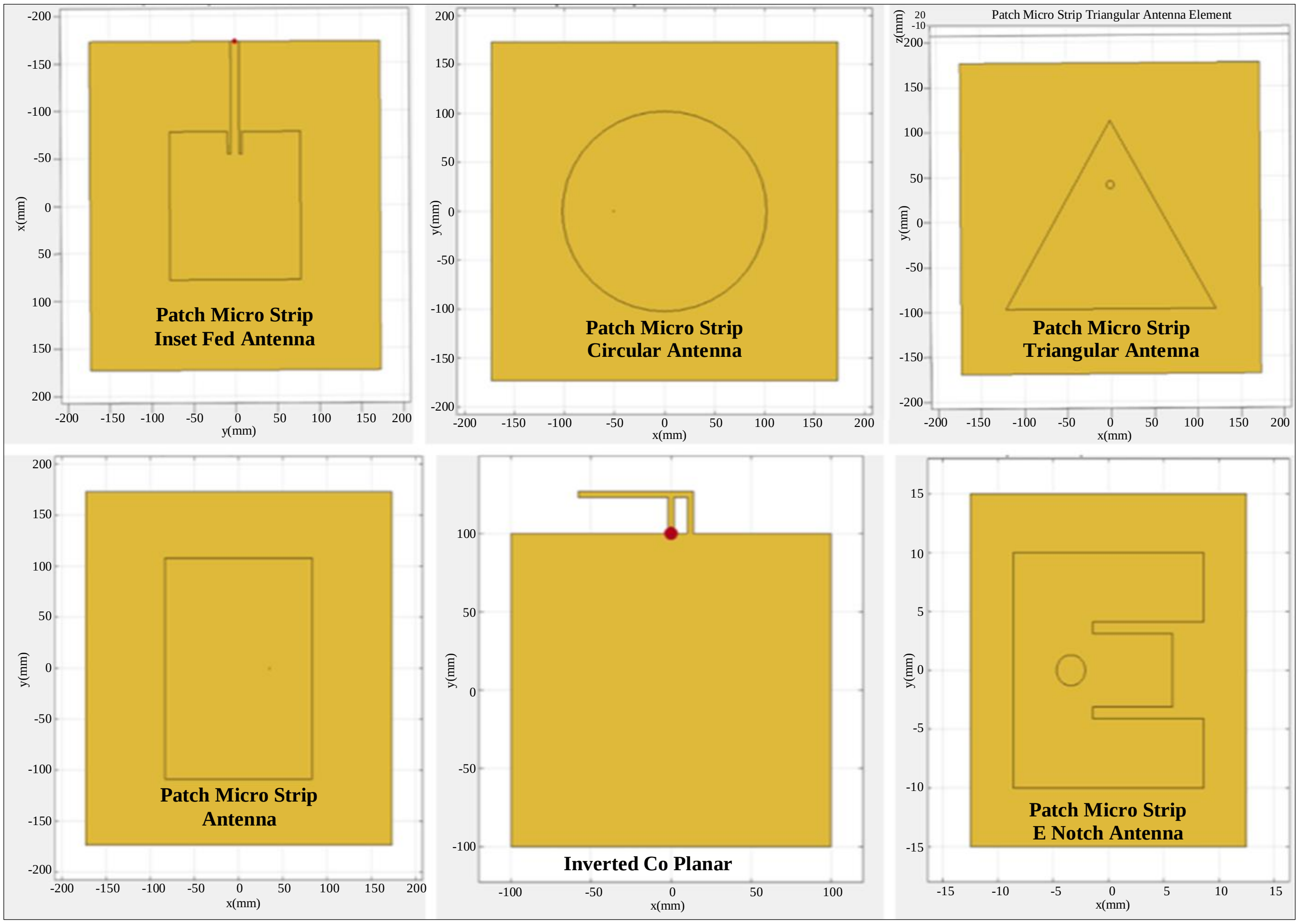

Fig. 2 Patch family antenna designed for experiment

Table 1. Antenna designed and analyzed for the experiment

Type of Antenna	Impedance	dB Value	Distribution
Patch Microstrip Element	-20 to +60	25 dB	High
Pifa Antenna	-100 to +100	13 dB	Low
Inverted F Co Planar	-100 to +200	16 dB	Low
Inverted L Co Planar	-50 to +50	9 dB	Low
Patch Micro Strip Circular	-50 to +150	8 dB	Low
Patch Micro Strip Inset fed	**-200 to +400**	**25 dB**	**High**

The design, fabrication, and pattern analysis of the antennas, such as the Pifa antenna, Micro strip element Antenna, Patch Microstrip inset Antenna, Patch Microstrip Circular Antenna, etc., are performed in real time to achieve better accuracy. Table 1 shows the analysis of antennas to finalize the radio frequency enabled antenna source. The experiment is conducted to choose the most suitable antenna for the proposed IoT positioning kit. Table 1 demonstrates that multiple antennas are manufactured, fine-tuned and optimized for the experiment.

It is evident from Table 1 that a patch micro inset fed antenna shall be considered for the set-up. The antenna selected has better impedance, dB range, and distribution than the others. Real time kinematics based positioning is a technique that performs positioning computation. The hardware integrates geodata receiver comprising Rover and Ranger stations and is communicated through the server. The IoT hardware device proposed is depicted as shown in Figure 4.

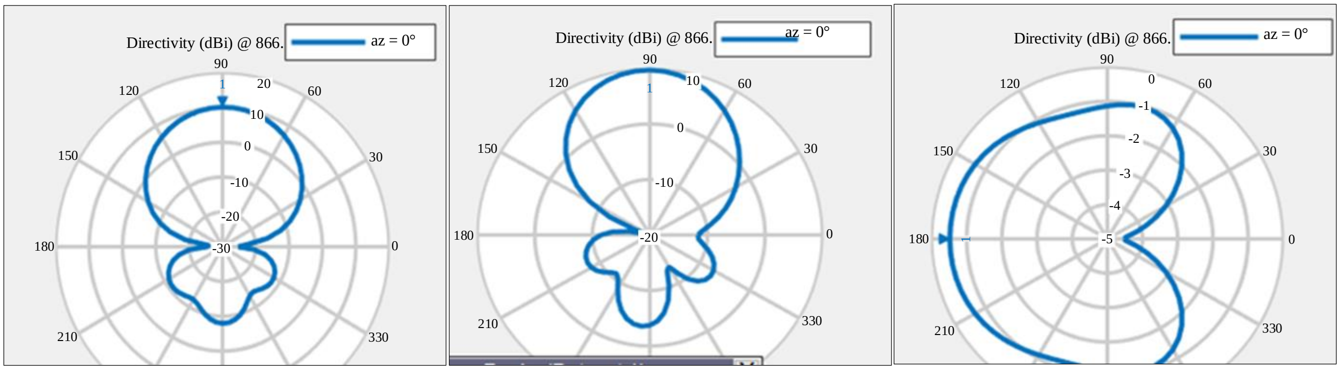

(a) Microstrip Antenna Coverage **(b) Patch Micro Strip Circular Coverage** **(c) Inverted F Co Planar Coverage**

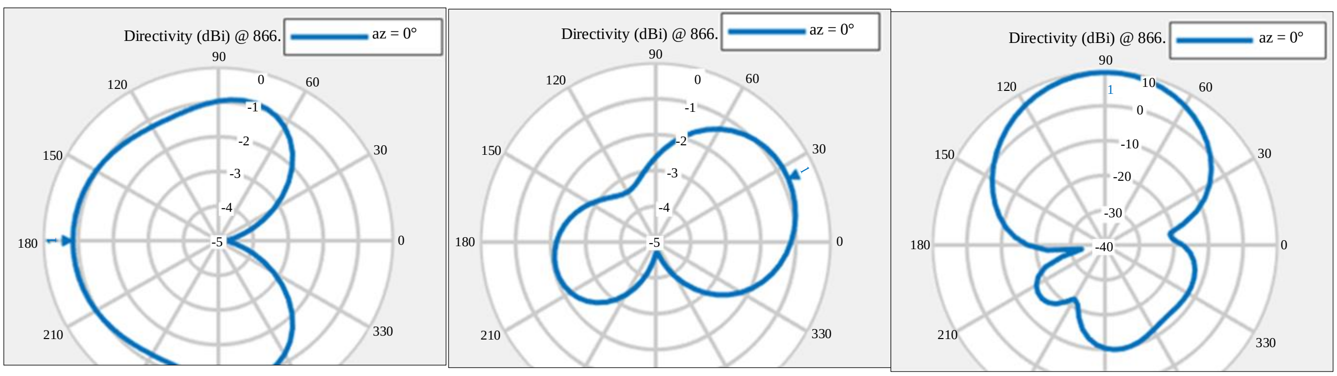

(d) Inverted L Co Planar Coverage **(e) Patch Micro Strip Inset Fed Coverage**

Fig. 3 Distribution coverage analysis of antennas

Fig. 4 IoT positioning kit placed at remote farmland

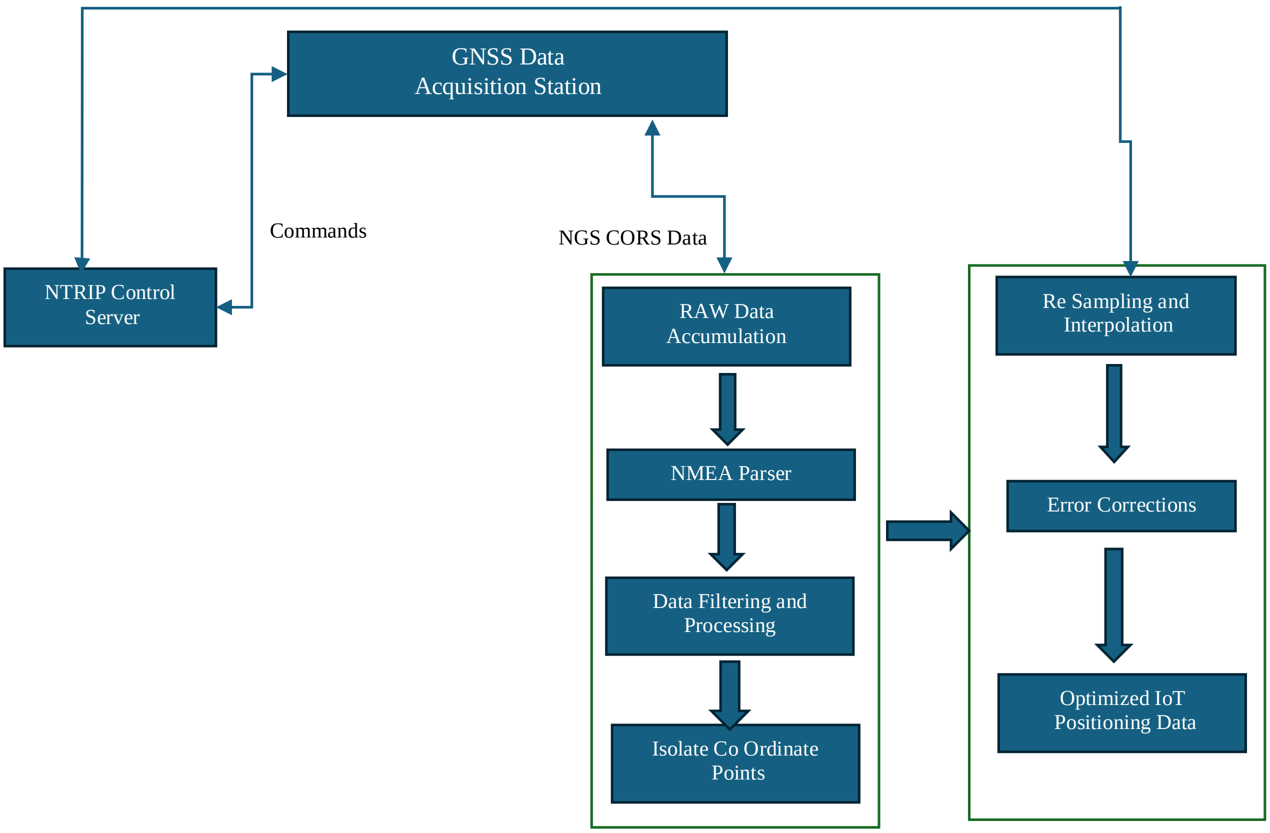

Fig. 5 Proposed solution

The proposed solution needs an IoT positioning kit, as shown in Figure 5. The positioning kit is placed in the remote area that is to be tracked. The IoT system is deployed in the locality identified and obtains data from satellites. The received raw data is finetuned further and is optimized dynamically at the edge server. The satellite response generated is extracted automatically once every 4 milliseconds and is displayed on mobile devices through an android application.

The process framework used in this paper to obtain precision accuracy is represented in Figure 5. The model consists of a CLI-driven control server, a Data Acquisition station, and User Services. The processing activities at the services interface consist of parsing logic with optimization, Isolating coordinate points, Interpreting and Correcting them, Generating new coordinate points, and finally, distributing data.

The satellite constellations that are in the range of are selected from the NTRIP control server. The satellite constellation scope is represented in Figure 6. The constellations that appear in green are the active satellites, and signals are captured to record the positioning data.

Figure 7 demonstrates the data received at the base station and rover station. The base station is fixed at the Tumakuru location, and the remote rover stance is fixed at Nelamanga district.

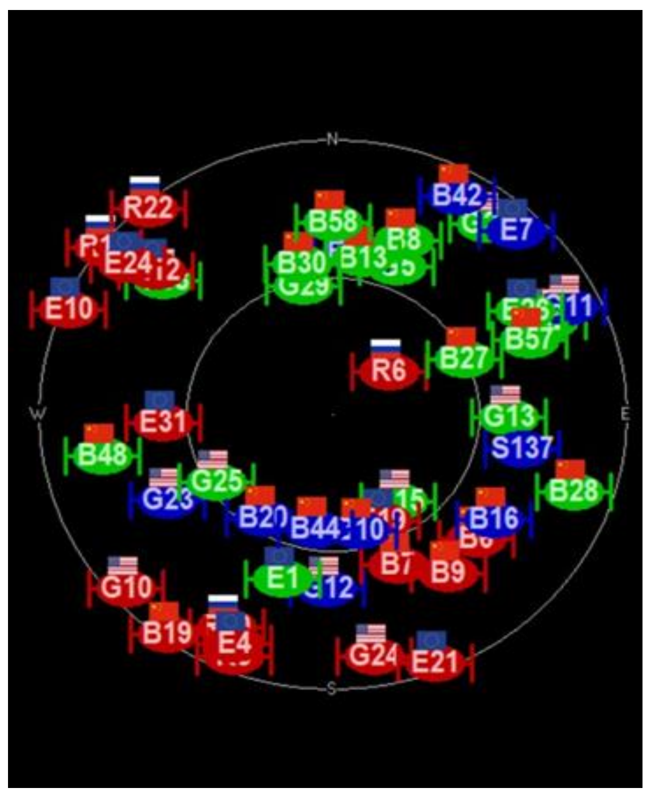

Fig. 6 Satellite constellations captured in simulator

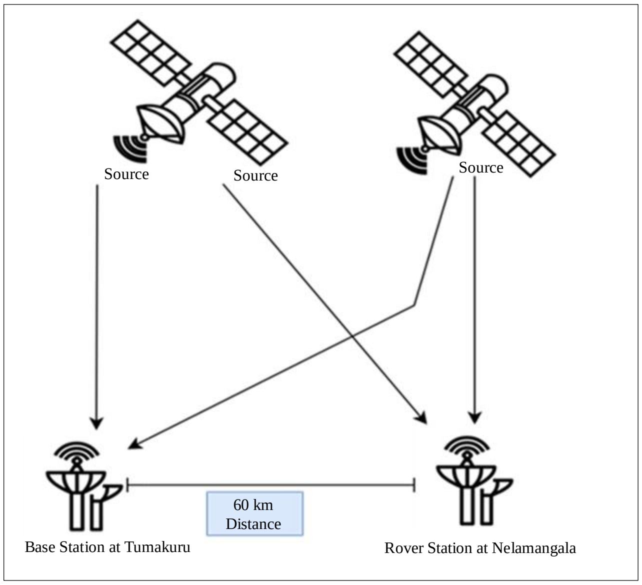

Fig. 7 Active satellite data transmission

The IoT device generates raw data for positioning, and the sample of the values received is shown in Figure 8. As shown in Figure 8, the distortions are caused by errors such as satellite clock bias, speed, multiple constellation paths, doppler effects, noise, etc.

The GNSS positing derivation is based on the simple mathematical formula depicted in Equation (1).

$$pt_i = \sqrt{(x - x_1)^2 + (y - y_1)^2 + (z - z_1)^2} \quad (1)$$

Where,
p is the speed of light
t_i travel time of satellite i
(x,y,z) and (x_1,y_1,z_1) co ordinates of GPS data.

Let us gather the raw data with distance records. After recording distance, every 4 seconds thereafter, record the elapsed time, t and distance, dist(t), until the final distance value is 1 cm. Let us consider the exponential function as shown in Equation (2).

$$dist(t) = Ee^{-pt} \quad (2)$$

Where E and e are the positive constants representing error correction value.

	Time	Global Positioning System FIXED	UTC coordinated	Latitude	Northing Indicator	Longitude	Easting Indicator	Status: 1D/2D	No of SVs used for navigatio	Horizontal Dillusion of Precision	Altitude	Metres	Geold Separation	Unit in Metres	Age of DGNSS correctio	V(t)	err
1	00:08:09	$GNGGA,	100809.00,	1319.308	N	7707.6131	E	1	12	0.8	841.6	M	-85.1	M	6C	861.7203	87.2
2	00:08:10	$GNGGA,	100810.00,	1319.308	N	7707.6131	E	1	12	0.8	841.8	M	-85.1	M	68	861.7619	84
3	00:08:11	$GNGGA,	100811.00,	1319.308	N	7707.6131	E	1	12	0.65	841.8	M	-85.1	M	66	861.8035	66.95
4	00:08:12	$GNGGA,	100812.00,	1319.308	N	7707.6130	E	1	12	0.65	841.9	M	-85.1	M	66	861.8452	66.95
5	00:08:13	$GNGGA,	100813.00,	1319.308	N	7707.6130	E	1	12	0.65	842.1	M	-85.1	M	6C	861.8868	70.85
6	00:08:14	$GNGGA,	100814.00,	1319.308	N	7707.6130	E	1	12	0.65	842.2	M	-85.1	M	6B	861.9285	70.2
7	00:08:15	$GNGGA,	100815.00,	1319.308	N	7707.6130	E	1	12	0.65	842.2	M	-85.1	M	69	861.9701	68.9
8	00:08:16	$GNGGA,	100816.00,	1319.308	N	7707.6130	E	1	12	0.8	842.4	M	-85.1	M	61	862.0118	78.4
9	00:08:17	$GNGGA,	100817.00,	1319.308	N	7707.6130	E	1	12	0.65	842.6	M	-85.1	M	64	862.0534	65.65
10	00:08:18	$GNGGA,	100818.00,	1319.308	N	7707.6130	E	1	12	0.65	842.7	M	-85.1	M	63	862.0951	65
11	00:08:19	$GNGGA,	100819.00,	1319.308	N	7707.6130	E	1	12	0.8	842.9	M	-85.1	M	6A	862.1367	85.6
12	00:08:20	$GNGGA,	100820.00,	1319.308	N	7707.6131	E	1	12	0.65	843.1	M	-85.1	M	64	862.1784	65.65
13	00:08:21	$GNGGA,	100821.00,	1319.308	N	7707.6131	E	1	12	0.65	843.3	M	-85.1	M	69	862.22	68.9
14	00:08:22	$GNGGA,	100822.00,	1319.308	N	7707.6130	E	1	12	0.8	843.3	M	-85.1	M	6F	862.2617	89.6
15	00:08:23	$GNGGA,	100823.00,	1319.308	N	7707.6130	E	1	12	0.65	843.3	M	-85.1	M	68	862.3033	68.25
16	00:08:24	$GNGGA,	100824.00,	1319.308	N	7707.6130	E	1	12	0.65	843.3	M	-85.1	M	60	862.345	63.05
17	00:08:25	$GNGGA,	100825.00,	1319.308	N	7707.6130	E	1	12	0.8	843.2	M	-85.1	M	67	862.3867	83.2
18	00:08:26	$GNGGA,	100826.00,	1319.308	N	7707.6130	E	1	12	0.65	843.3	M	-85.1	M	6E	862.4283	72.15
19	00:08:27	$GNGGA,	100827.00,	1319.308	N	7707.6130	E	1	12	0.65	843.4	M	-85.1	M	61	862.47	63.7
20	00:08:28	$GNGGA,	100828.00,	1319.308	N	7707.6129	E	1	12	0.8	843.4	M	-85.1	M	6A	862.5117	85.6
21	00:08:29	$GNGGA,	100829.00,	1319.308	N	7707.6130	E	1	12	0.65	843.6	M	-85.1	M	6C	862.5534	70.85
22	00:08:30	$GNGGA,	100830.00,	1319.308	N	7707.6131	E	1	12	0.65	843.9	M	-85.1	M	68	862.595	68.25
23	00:08:31	$GNGGA,	100831.00,	1319.308	N	7707.6131	E	1	12	0.8	844	M	-85.1	M	6A	862.6367	85.6
24	00:08:32	$GNGGA,	100832.00,	1319.308	N	7707.6131	E	1	12	0.76	844.1	M	-85.1	M	6A	862.6784	81.32
25	00:08:33	$GNGGA,	100833.00,	1319.308	N	7707.6130	E	1	12	0.76	844.1	M	-85.1	M	6E	862.7201	84.36

Fig. 8 Satellite data received continuously at remote location

Let E_r be the exponential spatial threshold value. Then, the Equation (1) is updated as shown in Equation (3).

$$dist(t) = Ee^{-pt} \quad + E_r \tag{3}$$

The initial recorded distance value is dist (0). Then, the deviation is calculated as per Equation (4).

$$dist(t) = (dist(0) - E_r)e^{-pt} \quad + E_r \tag{4}$$

If the function fits all of the data, then any of the ordered pairs should satisfy the function. For example, use pair (d/2, t/2) from the recorded data and the value of error correction constant p can be set with 0.01. Then, the distance amount can be derived as per Equation (5).

$$dist(t) = (d_0)e^{-0.01t} \quad + d_1 \tag{5}$$

The step is to be repeated to find the constant for all the pairs. Once the distance is determined, the time(t) vector can be determined as per the Equation (6).

$$time(t) = 2\pi \div \sqrt{E_r} \times dist_t \tag{6}$$

During the period time(t), the correlation variation per time is to be obtained as correction can be done by using a first-order linear equation. The coordination system points (x,y) are related by mapping functions obtained from the CORS data set (u,v) as given in Equation (7).

$$u = f(x, y, z) \quad and\ v = g(x, y, z) \tag{7}$$

The translation due to distortion is represented by 1st degree polynomial. The new value nth value of u and v for nth order coordinate sets $\{a_n, b_n\}$. The new coordinate system may not have one to one mapping with actual points. The actual to new coordinate difference can be calibrated and is dependent on the degree of the polynomial used in the mapping function, and the average mapping range is (n+1) (n+2)/2.

With resampling and interpolation, one can correct the misalignment and distortion. Furthermore, error correction and modeling can be done with the optimized computational procedure or technique. However, the Precision rate with respect to the inclination of coordinate system deviation varies due to distortion.

Let the wavelength displacement be Δʎ. The periodic repetition parameter with target positioning array Q can be obtained as shown in Equation (8).

$$Q = 1 + (K \div N) \times \Delta ʎ \tag{8}$$

Where,
K represents distortions observed,
N represents integer ambiguity.

The ratio K/N represents the successive deviation parameter. Generally, ambiguity is observed, and inaccurate distances are measured using the pseudo range technique. The ambiguity is calculated as a float number, and the mode is called float mode. One needs to identify the integer ambiguity around the float model. An accurate receiver position relative to the ranger, i.e., base station. If the integer ambiguity is corrected, the real time kinematics mode is set to Fixed mode.

The approximation is needed to get the precision accuracy of the land area. The back propagation based neural network method with an optimized Artificial Bee Colony algorithm is used in this paper to optimize the parameter, and the dynamic threshold technique is used to predict the future approximation of location points. As per the Bee Colony algorithm, the nearby coordinates are investigated, and further information is shared to engage new coordinates. Depending on the probability of value associated with the positioning source array is calculated. The Optimized Artificial Bee Colony algorithm logic is depicted in Figure 9.

Figure 9 represents the optimization logic used for the approximation of the positioning data. For correction and positioning accuracy, new approximation values are to be computed using the logic shown in Figure 8. The approximation is performed by applying a bee colony algorithm. The labels 1, 2 and 3 represent three active bee work.

Node 1 approximates the ranger area A and B's data. Node 2 represents fetching the details of positioning from sources A, and B. Node 3 receives the appropriate positioning data to the ranger. Operations such as fetch and share are performed while receiving data from the source location. We need to determine the phase signal as it depends on the distance between the ranger and the rover.

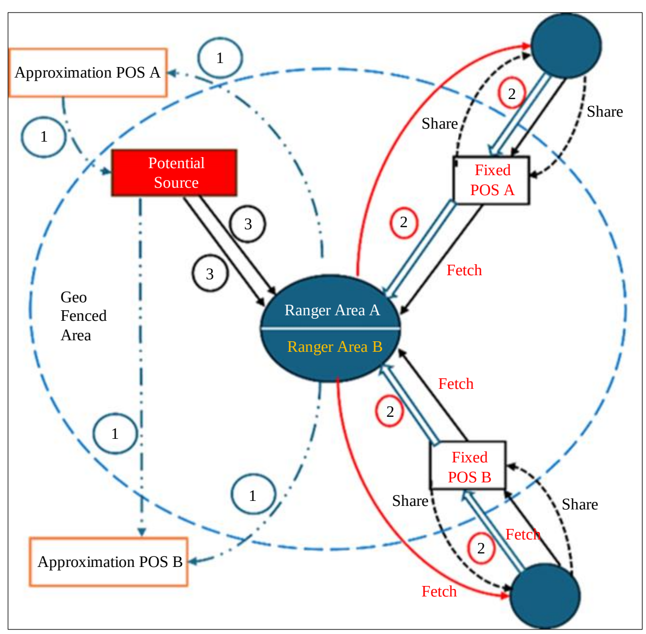

Fig. 9 Optimized artificial bee colony algorithm flow

```
Set the maximum number of error iterations e, i=1, j=1, t=0.4
For i=1, 1: N-1 do
    For j=1: Array of Distance do
        Do the random initialization before fetching the array, Q I, j.
        For E=1: e do
            if 0< Qi,j < 1-t
            e   Qe+1,j = Qe,j / (1-t)
            lse
                Qe+1, j = (Qi, j - 1, t) / t
            End if
        End For
    End for
End for
```

Fig. 10 Bee colony optimization logic

```
Step 1: Initialize the positioning parameters
Step 2: Generate the error count Qe+1, j
Step 3: Initialize bee colony sector nodes ni by ni,j = niminj+  eq (nimax - niminj )
Step 4: Measure the potential difference between each nodes
Step 5: Get the potential source nide as, best = nn
Step 6: Loop through each node
Step 7: Iterate through maxcount of nodes
            Calculate the approximate distance from each node4
Step 8: Calculate the potential value based on greedy colonization
Step 9: If selected node is updated then
            sharei = 0
        else
            sharei = sharei + 1
Step 10: if freqi< freqiesti then
            best = ni
          endif
End of iteration
Step 11: The potential source is updated by
            Niter + 2/(1+iter). Rand(nbest – niter) + 1/(1+iter) rand(nij
        End for
Output: The final output value
```

Fig. 11 Artificial bee colony optimization algorithm

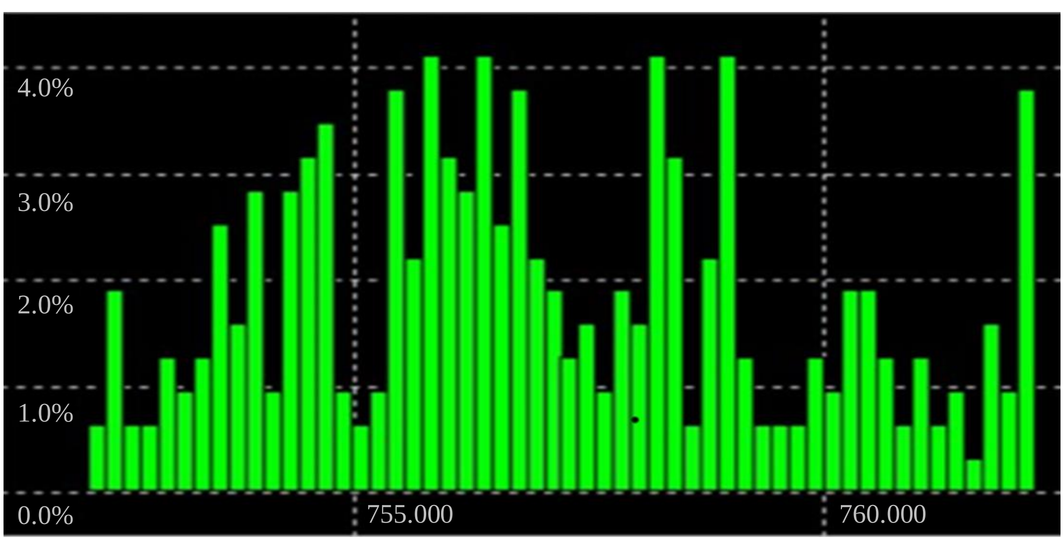

Fig. 12 Satellite data distortions captured

At ranger, the signal phase is measured for each active satellite and derived as shown in Equation (9).

$$A_{freq} \times B_{freq} = A_{amplitude}\, B_{amplitude} \div 2 \;\; [\cos(4\pi t(freq) \pm 2\pi \div \lambda)\, dist(t)] \quad (9)$$

Now, the optimized distance is derived from signal wavelengths and is obtained as per Equation (10).

$$dist_{new}(t) = N\,Q + (Phase_{rec} \div 2\pi) \quad (10)$$

Where,
N represents integer ambiguity
Q represents the positioning array

Then, the distance between two remote ends is calibrated as per Equation (11).

$$dist(Ranger_{A,i}) = 2\pi \div \lambda\, [dist_{new}(i)[\; - N_i\, \lambda + \mathrm{t}\,(satellite_i - Ranger_i) \quad (11)$$

Where,
λ is wavelength,
$dist_{new}(i)$ is the distance of the satellites,
N_i is integer ambiguity from received satellite I,
t is the speed of light.

The error measured for each satellite and ranger station is corrected and approximated. To understand the chaotic mapping between the ranges, an artificial bee colony is optimized as per the algorithm logic depicted in Figures 10 and 11.

4. Results and Discussion

4.1. Test Set Up and Environment

For testing, the RTK base station and RTK Rover station are set up at two different locations with a distance of upto 60km. Once the station is ready, the GNSS receivers start collecting the data. The signal received constitutes latitude, longitude, altitude, TIFF mode, Active Satellites and GNSS in fixed. Once the fixed mode is attained, the raw data is collected every 4 seconds. The resulting map is displayed with deviation details and with a precision accuracy of 100%, shown in Figure 11.

The received signals captured by the rover station and ranger station are calibrated further. The received signal contains distortions. The distortions observed are recorded, and the statistics of errors are shown in figure. The frequency distortion for every 5 sample differences and at the scale of 1 unit is depicted in Figure 12.

The statistics of the data received in one sampling period are shown in Figure 13. The summary of the parameters and the ranges for one iteration sample of the data cycle upto 20 ranges are depicted. The data was fetched continuously for 9 minutes at the remote location, Nelamangala and is monitored at the Tumakuru location. Based on the error correction statistics, the monitoring of the farmland is conducted continuously for a duration of upto 6 months. The data format is depicted in Figure 14. Data received in FIXED mode will fix the position values at the obtained latitude, longitude and altitude. The error corrections to latitude, longitude, altitude and diffusions are shown in Figure 16. The sampling of 4 nearest coordinate points is collected, and errors are identified for the approximation corrections.

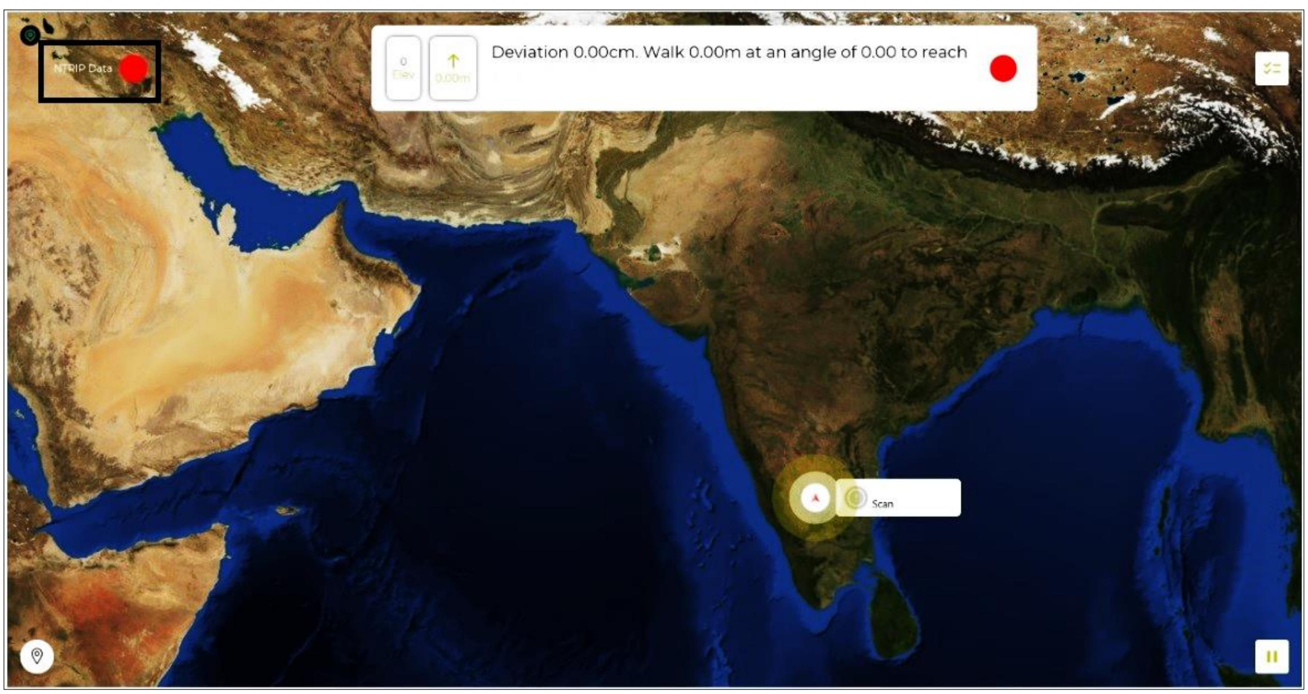

Fig. 13 Real time positioning fetched with cm

```
     ...1              Time                        Global Positioning System FIXED DATA UTC coordinated
Min.   :  1.0   Min.   :1899-12-31 00:08:09.00   Length:375                         Length:375
1st Qu.: 94.5   1st Qu.:1899-12-31 10:09:31.75   Class :character                   Class :character
Median :188.0   Median :1899-12-31 10:10:54.50   Mode  :character                   Mode  :character
Mean   :188.0   Mean   :1899-12-31 09:07:39.32
3rd Qu.:281.5   3rd Qu.:1899-12-31 10:12:17.25
Max.   :375.0   Max.   :1899-12-31 10:13:40.00
                NA's   :43
  Latitude          Northing Indicator  Longitude          Easting Indicator  Status: 1D/2D
Length:375         Length:375         Length:375         Length:375         Min.   :1
Class :character   Class :character   Class :character   Class :character   1st Qu.:1
Mode  :character   Mode  :character   Mode  :character   Mode  :character   Median :1
                                                                            Mean   :1
                                                                            3rd Qu.:1
                                                                            Max.   :1
                                                                            NA's   :43
No of SVs used for navigation Horizontal Dillusion of Precision    Altitude          Metres
Min.   :12                    Min.   :0.5900                  Min.   :837.3   Length:375
1st Qu.:12                    1st Qu.:0.6500                  1st Qu.:840.3   Class :character
Median :12                    Median :0.7000                  Median :842.0   Mode  :character
Mean   :12                    Mean   :0.7183                  Mean   :842.1
3rd Qu.:12                    3rd Qu.:0.7500                  3rd Qu.:843.8
Max.   :12                    Max.   :1.2100                  Max.   :847.3
NA's   :43                    NA's   :43                      NA's   :43
GeoId Separation Unit in Metres     Age of DGNSS correction and ID of reference station      V(t)
Min.   :-85.1    Length:375         Length:375                                           Min.   : 861.7
1st Qu.:-85.1    Class :character   Class :character                                     1st Qu.:4925.9
Median :-85.1    Mode  :character   Mode  :character                                     Median :4945.6
Mean   :-85.1                                                                            Mean   :4518.9
3rd Qu.:-85.1                                                                            3rd Qu.:4965.4
Max.   :-85.1                                                                            Max.   :4985.3
NA's   :43                                                                               NA's   :43
     err              ...19             ...20
Min.   :  0.00   Min.   :  0.00   Length:375
1st Qu.: 67.61   1st Qu.: 99.00   Class :character
Median : 72.80   Median :104.00   Mode  :character
Mean   : 71.41   Mean   : 98.49
3rd Qu.: 78.00   3rd Qu.:107.75
Max.   :131.89   Max.   :111.00
NA's   :25       NA's   :25
```

Fig. 14 Navigation data statistics

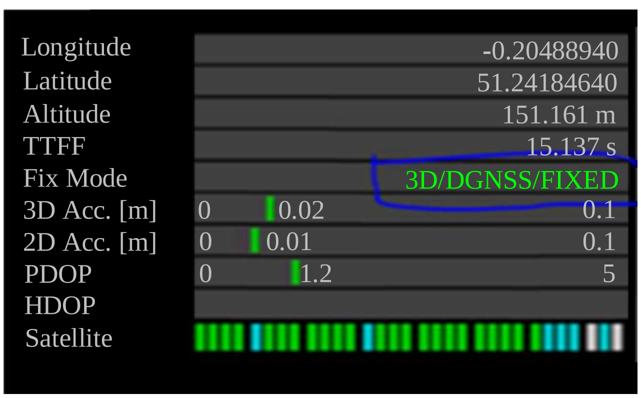

Fig. 1 Data received in FIXED mode

The navigation status is obtained from approximately 12 active satellites in TIFF format once FIXED mode is set. Throughout 0 to 9 minutes, the sampling data was collected from active satellites. The status of active satellites over timestamp is shown in Figure 15. The error correction statistics are shown in Figure 16. Errors for latitude, longitude, UTC values, altitude, and distributions are captured, and correction measures are carried out to approximate position values. Error corrections proposed in this paper are needed to fix the rover and ranger distortion values. The live positioning area of the farmland is captured remotely, as shown in Figure 17. The mean square error of the hyperparameter values collected for observed and estimated are analyzed as shown in Figure 18. The sampled error correction for the errors observed in the scale from 60 to 120 are rectified. Over 375 observations are made, and the precision status is shown in Figure 19.

At the end of the timestamp of the given target, the precision status with respect to diffusion is obtained and analyzed. At this point, the precision approximation is calibrated to the new source value as per the error correction algorithm proposed in the paper. The result shows that the precision accuracy of 100% is reached with the accuracy of 1cm in the target field, i.e., the agriculture field, as shown in figure. The randomness is observed in the initial iterations, and hence, accuracy is not easily achievable. Error correction is required to obtain precision accuracy in estimation. With the application of the Bee Colony algorithm, optimization of frequency through real time kinematics and tuning of inset fed antenna, errors are corrected. The Precision correction status is depicted in Figure 20.

The existing system for IoT real time positioning system uses GPS based methods. In this paper, it is proposed that GPS technology be used along with IoT, Real time kinematics, sensors, and GNSS. The comparative analysis of the existing method and the proposed method is shown in Table 2. Table 2 shows that the proposed method gives better accuracy than the existing positioning technologies.

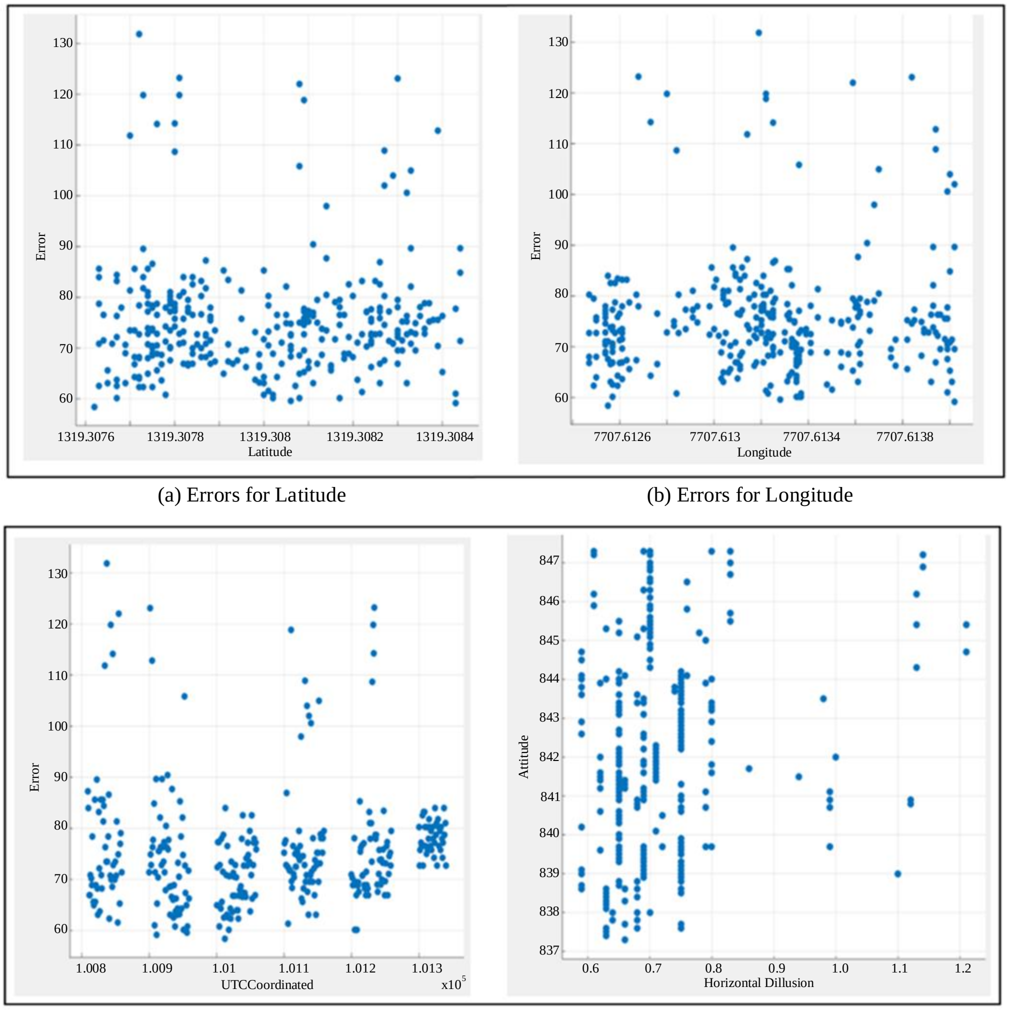

(a) Errors for Latitude (b) Errors for Longitude

(c) Errors for UTC Values (d) Errors for Altitude and Horizontal Dillusion

Fig. 16 Error corrections to be made for positioning approximation

Fig. 17 Real time positioning of farmland at cm accuracy

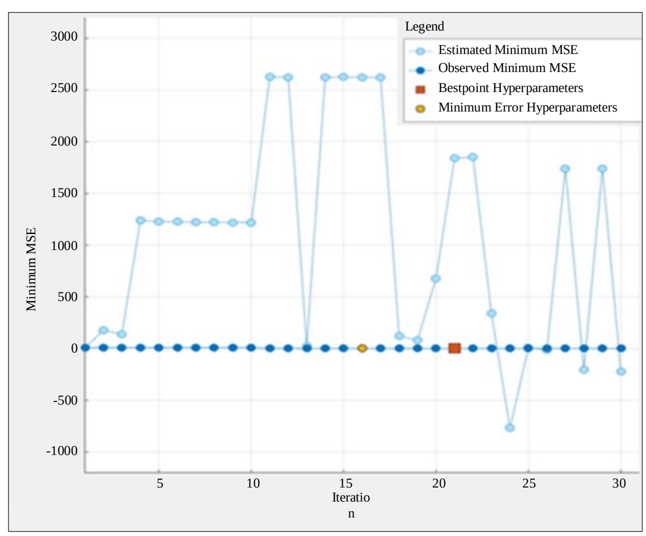

Fig. 18 Hyperparameters estimated vs observed

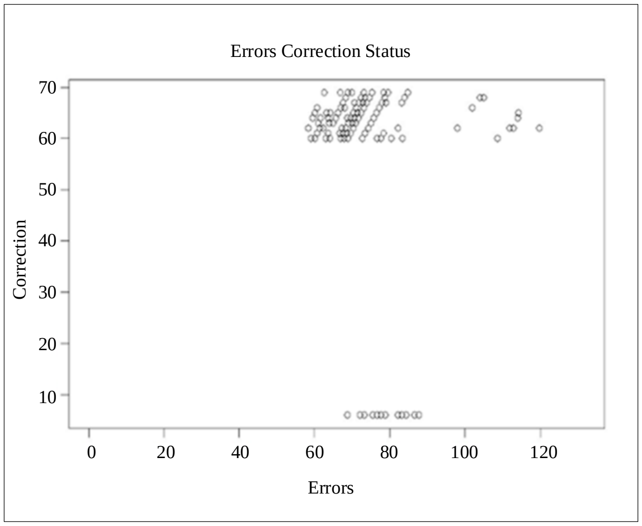

Fig. 19 Error correction status

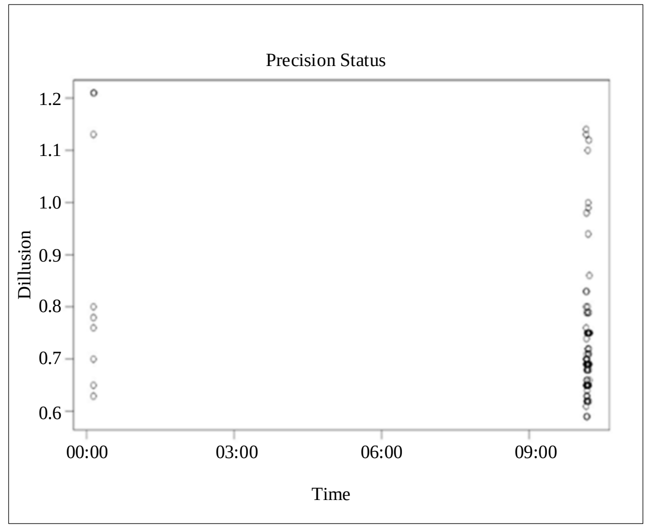

Fig. 20 Precision status

Table 2. Comparison analysis with respect to accuracy

Methods	Technology Used	Accuracy
GIS Approach	Geo Fencing	10m
Kriging Interpolation	Spatial Co-Variance Structure Sampling	5m
Proposed Method	IoT with GNSS and Real Time Kinematics	1cm

5. Conclusion

The application of IoT in the agriculture field is a need of the Indian agriculture sector today. Digitizing and remotely monitoring the crop area is required. In the paper, an accurate precision mechanism is proposed. The proposed method uses the sensor to detect the object in the field, and real time kinematics is integrated with GPS to locate the area precisely. As part of the research work, a tracker IoT kit is designed and built. The IoT consists of a sensor, inset fed antenna, integrated real time kinematics and GNSS receiver module and an application to trace the details. To correct the redundant data and errors received through signals from the navigation system, a novel optimized Artificial Bee Colony algorithm is implemented and used. With real time testing in the agriculture field, an accuracy of 99.9% is achieved with a cm level.

Funding Statement

CEDLabs Pvt. Ltd., Tumakuru, funded the work as part of the research work on real time positioning.

Acknowledgments

This research was supported by CEDLABS Pvt. Ltd., Tumakuru, Karnataka. I thank CEDLABS Pvt. Ltd. and the team members who provided insight and expertise that greatly assisted the research.

References

[1] James A. Slater, and Stephen Malys, "WGS 84 - Past, Present and Future," *Advances in Positioning and Reference Frames*, pp. 1-7, 1998. [CrossRef] [Google Scholar] [Publisher Link]

[2] Siyao Dang, Haisheng Huang, and Xin Li. "About the Parsing of NMEA-0183 Format Data Streams in GPS," *Advances in Natural Computation, Fuzzy Systems and Knowledge Discovery*, pp. 1282-1289, 2023. [CrossRef] [Google Scholar] [Publisher Link]

[3] Sungchan Jeong et al., "Tracking Diurnal to Seasonal Variations of Gross Primary Productivity Using a Geostationary Satellite, GK-2A Advanced Meteorological Imager," *Remote Sensing of Environment*, vol. 284, 2023. [CrossRef] [Google Scholar] [Publisher Link]

[4] Wanxin Xiao et al., "An Automated Algorithm to Retrieve the Location and Depth of Supraglacial Lakes from ICESat-2 ATL03 Data," *Remote Sensing of Environment*, vol. 298, 2023. [CrossRef] [Google Scholar] [Publisher Link]

[5] David Vieira et al., "Positioning and Attitude Determination for Precision Agriculture Robots Based on IMU and Two RTK GPSs Sensor Fusion," *IFAC-Papers on Line*, vol. 55, no. 32, pp. 60-65, 2022. [CrossRef] [Google Scholar] [Publisher Link]

[6] Anam M. Khan et al., "Reviews and Syntheses: Ongoing and Emerging Opportunities to Improve Environmental Science Using Observations from the Advanced Baseline Imager on the Geostationary Operational Environmental Satellites," *Biogeosciences*, vol. 18, no. 13, pp. 4117-4141, 2021. [CrossRef] [Google Scholar] [Publisher Link]

[7] Agata M. Wijata et al., "Taking Artificial Intelligence into Space through Objective Selection of Hyperspectral Earth Observation Applications: To bring the "Brain" Close to the "Eyes" of Satellite Missions," *IEEE Geoscience and Remote Sensing Magazine*, vol. 11, no. 2, pp. 10-39, 2023. [CrossRef] [Google Scholar] [Publisher Link]

[8] M. Bietresato et al., "A Tracked Mobile Robotic Lab for Monitoring the Plants Volume and Health," *2016 12th IEEE/ASME International Conference on Mechatronic and Embedded Systems and Applications (MESA)*, Auckland, New Zealand, pp. 1-6, 2016. [CrossRef] [Google Scholar] [Publisher Link]

[9] André Silva Aguiar et al., "Localization and Mapping for Robots in Agriculture and Forestry: A Survey," *Robotics*, vol. 9, no. 4, 2020. [CrossRef] [Google Scholar] [Publisher Link]

[10] Tomoaki Miura et al., "Improved Characterization of Vegetation and Land Surface Seasonal Dynamics in Central Japan with Himawari-8 Hyper Temporal Data," *Scientific Reports*, vol. 9, 2019. [CrossRef] [Google Scholar] [Publisher Link]

[11] Norman Kerle et al., "UAV-Based Structural Damage Mapping: A Review," *ISPRS International Journal of Geo-Information*, vol. 9, no. 1, 2020. [CrossRef] [Google Scholar] [Publisher Link]

[12] Berkay Bahadur, "Real-Time Single-Frequency Precise Positioning with Galileo Satellites," *The Journal of Navigation*, vol. 75, no. 1, pp. 124-140, 2022. [CrossRef] [Google Scholar] [Publisher Link]

[13] Nicola Angelo Famiglietti et al., "A Test on the Potential of a Low Cost Unmanned Aerial Vehicle RTK/PPK Solution for Precision Positioning," *Sensors*, vol. 21, no. 11, 2021. [CrossRef] [Google Scholar] [Publisher Link]

[14] Farzaneh Zangenehnejad, and Yang Gao, "GNSS Smartphones Positioning: Advances, Challenges, Opportunities, and Future Perspectives," *Satellite Navigation*, vol. 2, 2021. [CrossRef] [Google Scholar] [Publisher Link]

[15] Cong Khai Pham et al., "Research and Development of Real-time High-precision GNSS Receivers: A Feasible Application for Surveying and Mapping in Vietnam," *Journal of the Polish Mineral Engineering Society*, vol. 1, no. 2, pp. 391-404, 2021. [CrossRef] [Google Scholar] [Publisher Link]

[16] Yang Ye et al., "A Feasible Framework to Downscale NPP-VIIRS Nighttime Light Imagery Using Multi-Source Spatial Variables and Geographically Weighted Regression," *International Journal of Applied Earth Observation and Geoinformation*, vol. 104, 2021. [CrossRef] [Google Scholar] [Publisher Link]

[17] Guangtong Xu et al., "Trust-Region Filtered Sequential Convex Programming for Multi-UAV Trajectory Planning and Collision Avoidance," *ISA Transactions*, vol. 128, Part B, pp. 664-676, 2022. [CrossRef] [Google Scholar] [Publisher Link]

[18] Fabio Marcelo Breunig et al., "Delineation of Management Zones in Agricultural Fields Using Cover-Crop Biomass Estimates from PlanetScope Data," *International Journal of Applied Earth Observation and Geoinformation*, vol. 85, 2020. [CrossRef] [Google Scholar] [Publisher Link]

[19] Kathryn Elmer, and Margaret Kalacska, "A High-Accuracy GNSS Dataset of Ground Truth Points Collected within Iles-de-Boucherville National Park, Quebec, Canada," *Data*, vol. 6, no. 3, 2021. [CrossRef] [Google Scholar] [Publisher Link]

[20] Davis Dinkov, and Atanas Kitev, "Advantages, Disadvantages and Applicability of GNSS Post-Processing Kinematic (PPK) Method for Direct Georeferencing of UAV Images," *Proceedings of the 8th International Conference on Cartography and GIS*, Nessebar, Bulgaria, vol. 1, pp. 747-759, 2020. [Google Scholar]

[21] Yulong Ge et al., "An Analysis of BDS-3 Real-Time PPP: Time Transfer, Positioning, and Tropospheric Delay Retrieval," *Measurement*, vol. 172, 2021. [CrossRef] [Google Scholar] [Publisher Link]

[22] Jacek Paziewski et al., "An Analysis of Multi-GNSS Observations Tracked by Recent Android Smartphones and Smartphone-only Relative Positioning Results," *Measurement*, vol. 175, 2021. [CrossRef] [Google Scholar] [Publisher Link]

[23] Dengshuai Chen et al., "The Delineation of Ecological Redline Area for Catchment Sustainable Management from the Perspective of Ecosystem Services and Social Needs: A Case Study of the Xiangjiang Watershed, China," *Ecological Indicators*, vol. 121, 2021. [CrossRef] [Google Scholar] [Publisher Link]

[24] M.H.N. Talib et al., "An Improved Simplified Rules Fuzzy Logic Speed Controller Method Applied for Induction Motor Drive," *ISA Transactions*, vol. 105, pp. 230-239, 2020. [CrossRef] [Google Scholar] [Publisher Link]

[25] Weicheng Xu et al., "Cotton Yield Estimation Model Based on Machine Learning Using Time Series UAV Remote Sensing Data," *International Journal of Applied Earth Observation and Geoinformation*, vol. 104, 2021. [CrossRef] [Google Scholar] [Publisher Link]

[26] Yong Ge et al., "Geoscience-Aware Deep Learning: A New Paradigm for Remote Sensing," *Science of Remote Sensing*, vol. 5, 2022. [CrossRef] [Google Scholar] [Publisher Link]

[27] Mark Bolinger, and Greta Bolinger, "Land Requirements for Utility-Scale PV: An Empirical Update on Power and Energy Density," *IEEE Journal of Photovoltaics*, vol. 12, no. 2, pp. 589-594, 2022. [CrossRef] [Google Scholar] [Publisher Link]

[28] Yali Zhang, and Mingshi Li, "A New Method for Monitoring Start of Season (SOS) of Forest Based on Multisource Remote Sensing," *International Journal of Applied Earth Observation and Geoinformation*, vol. 104, 2021. [CrossRef] [Google Scholar] [Publisher Link]

[29] Yi He et al., "A Unified Network of Information Considering Superimposed Landslide Factors Sequence and Pixel Spatial Neighbourhood for Landslide Susceptibility Mapping," *International Journal of Applied Earth Observation and Geoinformation*, vol. 104, 2021. [CrossRef] [Google Scholar] [Publisher Link]

[30] Andreas A. Beckert et al., "The Three-Dimensional Structure of Fronts in Mid-Latitude Weather Systems in Numerical Weather Prediction Models," *Geoscientific Model Development*, vol. 16, no. 15, pp. 4427-4450, 2023. [CrossRef] [Google Scholar] [Publisher Link]

[31] Huidi Wang et al., "The Relaxed Implicit Randomized Algebraic Reconstruction Technique for Curve and Surface Reconstruction," *Computers & Graphics*, vol. 102, pp. 9-17, 2022. [CrossRef] [Google Scholar] [Publisher Link]

[32] A.H. Mazinan, and M. Shahi, "On High-Resolution Manoeuvres Control via Trajectory Optimization," *Sadhana*, vol. 42, pp. 245-255, 2017. [CrossRef] [Google Scholar] [Publisher Link]

[33] Qun Ma et al., "Spatial Scaling of Urban Impervious Surfaces across Evolving Landscapes: From Cities to Urban Regions," *Landscape and Urban Planning*, vol. 175, pp. 50-61, 2018. [CrossRef] [Google Scholar] [Publisher Link]

[34] Xuebin Yang et al., "Mapping Forest in the Southern Great Plains with ALOS-2 PALSAR-2 and Landsat 7/8 Data," *International Journal of Applied Earth Observation and Geoinformation*, vol. 104, 2021. [CrossRef] [Google Scholar] [Publisher Link]

[35] Piyapong Suwanno et al., "GIS-Based Identification and Analysis of Suitable Evacuation Areas and Routes in Flood-Prone Zones of Nakhon Si Thammarat Municipality," *IATSS Research*, vol. 47, no. 3, pp. 416-431, 2023. [CrossRef] [Google Scholar] [Publisher Link]

[36] Andre Broekman, and Petrus Johannes Grabe, "A Low-Cost, Mobile Real-Time Kinematic Geolocation Service for Engineering and Research Applications," *HardwareX*, vol. 10, 2021. [CrossRef] [Google Scholar] [Publisher Link]

[37] Bumairiyemu Maimaiti et al., "Urban Spatial Expansion and Its Impacts on Ecosystem Service Value of Typical Oasis Cities around Tarim Basin, Northwest China," *International Journal of Applied Earth Observation and Geoinformation*, vol. 104, 2021. [CrossRef] [Google Scholar] [Publisher Link]

[38] Feng Yang, and Zhenzhong Zeng, "Refined Fine-Scale Mapping of Tree Cover Using Time Series of Planet-NICFI and Sentinel-1 Imagery for Southeast Asia (2016–2021)," *Earth System Science Data*, vol. 15, no. 9, pp. 4011-4021, 2023. [CrossRef] [Google Scholar] [Publisher Link]

[39] Cheng Zhong et al., "Landslide Mapping with Remote Sensing: Challenges and Opportunities," *International Journal of Remote Sensing*, vol. 41, no. 4, pp. 1555-1581, 2019. [CrossRef] [Google Scholar] [Publisher Link]

[40] Yuri Taddia et al., "Quality Assessment of Photogrammetric Models for Façade and Building Reconstruction Using DJI Phantom 4 RTK," *Remote Sensing*, vol. 12, no. 19, 2020. [CrossRef] [Google Scholar] [Publisher Link]

[41] Vinod Singh Jadon, and K.P. Ray, "Analysis of Harmonics and Their Mitigation for a Tuned Cylindrical Monopole Antenna," *Sadhana*, vol. 48, 2023. [CrossRef] [Google Scholar] [Publisher Link]

[42] Prithish Chand et al., "Low-Profile Compact Printed Monopole Antenna for Satellite-Bas1ed AIS Application," *Defence Science Journal*, vol. 70, no. 2, pp. 175-182, 2020. [CrossRef] [Google Scholar] [Publisher Link]

[43] Moritz K. Lehmann et al., "Analysis of Recurring Patchiness in Satellite-Derived Chlorophyll a to Aid the Selection of Representative Sites for Lake Water Quality Monitoring," *International Journal of Applied Earth Observation and Geoinformation*, vol. 104, 2021. [CrossRef] [Google Scholar] [Publisher Link]

[44] Finu Shrestha et al., "A Comprehensive and Version-Controlled Database of Glacial Lake Outburst Floods in High Mountain Asia," *Earth System Science Data*, vol. 15, no. 9, pp. 3941-3961, 2023. [CrossRef] [Google Scholar] [Publisher Link]

[45] Nico Lang et al., "A High-Resolution Canopy Height Model of the Earth," *Nature Ecology & Evolution*, vol. 7, pp. 1778-1789, 2023. [CrossRef] [Google Scholar] [Publisher Link]

[46] David P. Roy et al., "A Global Analysis of the Temporal Availability of PlanetScope High Spatial Resolution Multi-Spectral Imagery," *Remote Sensing of Environment*, vol. 264, 2021. [CrossRef] [Google Scholar] [Publisher Link]

[47] Ruben Ferrer Velasco et al., "Towards Accurate Mapping of Forest in Tropical Landscapes: A Comparison of Datasets on how Forest Transition Matters," *Remote Sensing of Environment*, vol. 274, 2022. [CrossRef] [Google Scholar] [Publisher Link]

[48] Jingfeng Xiao et al., "Emerging Satellite Observations for Diurnal Cycling of Ecosystem Processes," *Nature Plants*, vol. 7, pp. 877-887, 2021. [CrossRef] [Google Scholar] [Publisher Link]

[49] Joe Breen et al., "POWDER: Platform for Open Wireless Data-Driven Experimental Research," *Proceedings of the 14th International Workshop on Wireless Network Testbeds, Experimental Evaluation and Characterization (WiNTECH)*, pp. 17-24, 2020. [CrossRef] [Google Scholar] [Publisher Link]

[50] Cong Miao, and Yu Wang, "Interpolation of Non-Stationary Geo-Data Using Kriging with Sparse Representation of Covariance Function," *Computers and Geotechnics*, vol. 169, 2024. [CrossRef] [Google Scholar] [Publisher Link]

[51] Yu Yao et al., "Egocentric Vision-Based Future Vehicle Localization for Intelligent Driving Assistance Systems," *2019 International Conference on Robotics and Automation (ICRA)*, Montreal, QC, Canada, pp. 9711-9717, 2019. [CrossRef] [Google Scholar] [Publisher Link]

[52] Mahek Vyas et al., "Implementation and Testing of Single Point Positioning on IRNSS/NavIC Receiver Data," *International Journal of Communication Systems*, vol. 37, no. 13, 2024. [CrossRef] [Google Scholar] [Publisher Link]

[53] Xingzhi Chang et al., “Design of a 3D Space Early Warning System for High Precision Positioning Technology of Beidou and Analysis of Differential Positioning Accuracy,” *Measurement: Sensors*, vol. 33, 2024. [CrossRef] [Google Scholar] [Publisher Link]

[54] Nandakumaran Nadarajah et al., “The Mixed-Receiver BeiDou Inter-Satellite-Type Bias and its Impact on RTK Positioning,” *GPS Solutions*, vol. 19, pp. 357-368, 2015. [CrossRef] [Google Scholar] [Publisher Link]

[55] Brian Paden et al., “A Survey of Motion Planning and Control Techniques for Self-Driving Urban Vehicles,” *IEEE Transactions on Intelligent Vehicles*, vol. 1, no. 1, pp. 33-55, 2016. [CrossRef] [Google Scholar] [Publisher Link]

[56] Tarik Kazaz et al., “Delay Estimation for Ranging and Localization Using Multiband Channel State Information,” *IEEE Transaction on Wireless Communications*, vol. 21, no. 4, pp. 2591-2607, 2022. [CrossRef] [Google Scholar] [Publisher Link]

[57] Nitin Kumar Vishwakarma, Ragini Shukla, and Ravi Mishra, “A Review of Different Methods for Implementing Smart Agriculture on An IoT Platform,” *SSRG International Journal of Computer Science and Engineering*, vol. 7, no. 12, pp. 5-8, 2020. [CrossRef] [Google Scholar] [Publisher Link]

[58] Ahmed Salim, Ahmed M. Khedr, and Walid Osamy, “Enhancing IoT-Enabled Sustainable Smart Cities with Secure and Energy-Aware Data Collection Using Meta-Heuristic Technique,” *IEEE Sensors Journal*, vol. 24, no. 14, pp. 22974-22991, 2024. [CrossRef] [Google Scholar] [Publisher Link]

[59] Denes Farago, Balint Maczak, and Zoltan Gingl, “Enhancing Accuracy in Actigraphic Measurements: A Lightweight Calibration Method for Triaxial Accelerometers,” *IEEE Access*, vol. 12, pp. 38102-38111, 2024. [CrossRef] [Google Scholar] [Publisher Link]

[60] Jayson P. Van Marter et al., “A Multichannel Approach and Testbed for Centimeter-Level WiFi Ranging,” *IEEE Journal of Indoor and Seamless Positioning and Navigation*, vol. 2, pp. 76-91, 2024. [CrossRef] [Google Scholar] [Publisher Link]

[61] Haiyun Yao et al., “A Benchmark of Absolute and Relative Positioning Solutions in GNSS Denied Environments,” *IEEE Internet of Things Journal*, vol. 11, no. 3, pp. 4243-4273, 2024. [CrossRef] [Google Scholar] [Publisher Link]

[62] Chandni Bajaj et al., “GPS-Integrated RFID Antenna with AMC Backing for IoT-Based Sensing and Tracking Applications,” *IEEE Transactions on Antennas and Propagation*, vol. 72, no. 2, pp. 1929-1934, 2024. [CrossRef] [Google Scholar] [Publisher Link]

[63] Maria Bermudez Arboleda et al., “Orientation Aware Intelligent 3-D Cubic Antenna System with Automated Radiation Pattern Reconfigurability,” *IEEE Open Journal of Antennas and Propagation*, vol. 3, pp. 812-823, 2022. [CrossRef] [Google Scholar] [Publisher Link]